Elasticity and magnetocaloric effect in $MnFe_4Si_3$

M. Herlitschke,[1,2,3,*] B. Klobes,[2] I. Sergueev,[1] P. Hering,[2] J. Perßon,[2] and R. P. Hermann[2,3,4,†]

[1]*FS-PE, Deutsches Elektronen-Synchrotron (DESY), D-22607 Hamburg, Germany*

[2]*Jülich Centre for Neutron Science JCNS and Peter Grünberg Institut PGI, JARA-FIT, Forschungszentrum Jülich GmbH, D-52425 Jülich, Germany*

[3]*Faculté des Sciences, Université de Liège, B-4000 Liège, Belgium*

[4]*Materials Science and Technology Division, Oak Ridge National Laboratory, Oak Ridge, Tennessee 37831, USA*

(Received 26 October 2015; revised manuscript received 19 January 2016; published 16 March 2016)

The room temperature magnetocaloric material $MnFe_4Si_3$ was investigated with nuclear inelastic scattering (NIS) and resonant ultrasound spectroscopy (RUS) at different temperatures and applied magnetic fields in order to assess the influence of the magnetic transition and the magnetocaloric effect on lattice dynamics. The NIS data give access to phonons with energies above 3 meV, whereas RUS probes the elasticity of the material in the MHz frequency range and thus low-energy, $\sim$ neV, phonon modes. A significant influence of the magnetic transition on the lattice dynamics is observed only in the low-energy, long-wavelength limit. $MnFe_4Si_3$ and other compounds in the $Mn_{5-x}Fe_xSi_3$ series were also investigated with vibrating sample magnetometry, resistivity measurements, and Mössbauer spectroscopy in order to study the magnetic transitions and to complement the results obtained on the lattice dynamics.

DOI: 10.1103/PhysRevB.93.094304

I. INTRODUCTION

The magnetocaloric effect (MCE), which refers to the reversible temperature change of a material upon application or removal of a magnetic field, is under investigation for room temperature refrigeration due to energy saving opportunities and the elimination of environmentally unfriendly gaseous refrigerants [1–3]. Although the MCE was discovered in 1881 by Warburg [4] and first used for ultralow temperature cooling over 80 years ago [5], research on room temperature applications intensified after 1997 with the discovery of the giant MCE in $Gd_5(Ge_2Si_2)$ close to room temperature and the related possible energy savings of up to 30% [2].

The MCE is thermodynamically described by an adiabatic process in which a change in the magnetic entropy leads to a change in the lattice entropy [3]. Neglecting the nuclear contribution, the total entropy is the sum of magnetic, lattice, and electronic entropy, which depends on temperature, magnetic induction, and pressure [6].

The magnitude of the MCE is usually determined by macroscopic methods, such as heat capacity and magnetometry [7]. Extracting the MCE from these measurements relies on the assumption that the overall entropy change is zero and the magnetic and the lattice entropy can be directly linked, neglecting the influence of conduction electrons. Note that the impact of electron-electron interactions on the MCE, especially in transition metal-based compounds, remains poorly understood [6].

The aim of this report is a detailed investigation of the MCE in the $MnFe_4Si_3$ compound and of the interplay between magnetism and lattice dynamics, which leads to a change of lattice entropy under applied magnetic field. For this purpose, the $Mn_{5-x}Fe_xSi_3$ series is particularly interesting because the volume change due to the magnetic transition is quite small (see Refs. [8,9] or the Supplemental Material [10]). This small change in volume allows for synthesizing single crystals without breaking and cracking upon crossing the transition temperature, as usually observed for other MCE materials with a first-order transition [11].

$Mn_{5-x}Fe_xSi_3$ compounds crystallize in the $P6_3/mcm$ structure (see Fig. 1). Fe and Mn are distributed on two different sites, i.e., the 4*d* and 6*g* sites. The metal atoms on the 4*d* site are coordinated by two other metals, stacked in the *c* direction, and six Si as nearest neighbors, at a distance of $\approx$2.38 Å, for $x = 4$. The metal atoms on the 6*g* site are organized in triangular units in the *ab* plane, with $\approx$2.75 Å interatomic distance. These triangular units are separated by $\approx$2.848 Å from those above and below in the *c* direction and stacked in a staggered mode.

The 4*d* and 6*g* sites of this solid solution can be occupied by Fe and Mn with a preferential site occupation, as shown by XRD and Mössbauer spectroscopy [12,14]. Iron tends to occupy the 4*d* site first. In the $x = 1$ compound, the 4*d* site has mixed iron and manganese occupation, whereas almost no iron occupies the 6*g* site. With increasing iron content, the 6*g* site also accommodates iron and starting from $x > 2$ the 4*d* site is almost fully occupied by iron and the 6*g* site has mixed occupation. This behavior was attributed to the more electronegative Fe forming more stable metal-metal bonds in the 4*d* site than Mn [14]. It was further reported that the lattice parameter and the unit cell volume become smaller with increasing iron content [14].

Recent results [8,9] indicate that this crystal structure is only approximate, because the metal sites are split with different occupations. However, for the following data analysis, the approximation of the $P6_3/mcm$ structure is a useful simplification.

II. EXPERIMENTAL

A. Sample preparation

$Mn_{5-x}Fe_xSi_3$ powder samples enriched to >90% with iron-57 were produced with $x = 1,2,3$, and 4 by induction melting

*marcus.herlitschke@desy.de
†hermannrp@ornl.gov

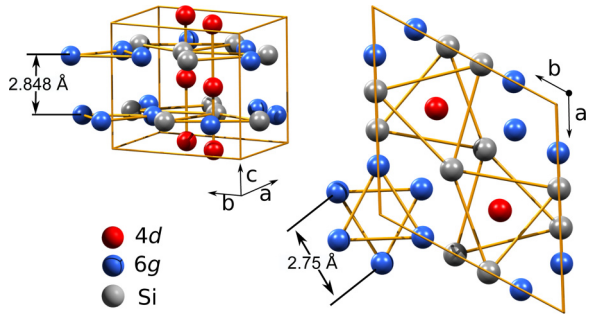

FIG. 1. The $P6_3/mcm$ unit cell of the $Mn_{5-x}Fe_xSi_3$ series [12,13]. The occupation of the 4*d* and 6*g* site changes with iron content.

in an inert Ar atmosphere. The obtained polycrystalline pellets, with a mass of roughly 100 mg, were thoroughly ground to powder. Natural isotopic abundance $MnFe_4Si_3$ powder with a mass of 100 g was produced in the same way for subsequent crystal growth with the Czochralski method, at a growth rate of 15 mm/h. The obtained single crystal was oriented by Laue diffraction, cut by spark erosion and polished.

B. Magnetometry, resonant ultrasound spectroscopy, and resistivity measurements

Magnetometry, resonant ultrasound spectroscopy (RUS) [15], and resistivity measurements were carried out in a Quantum Design physical properties measurement system (PPMS).

Magnetization was measured using vibrating sample magnetometry (VSM) on enriched and nonenriched powder samples. All measurements were performed with the zero-field cooled (ZFC) procedure. The magnetic entropy change was extracted from hysteresis curves according to Ref. [7], using the Maxwell relation,

$$\left(\frac{\delta S_m(T,B)}{\delta B}\right)_{T,p} = \left(\frac{\delta M(T,B)}{\delta T}\right)_{B,p}.$$

Resistivity and RUS measurements were performed using a polished single crystal of $MnFe_4Si_3$ with the standard resistivity option of the PPMS and a self-developed inset for RUS measurements. For in-field RUS, the *c* axis of the crystal was aligned parallel to the magnetic field. The crystal was cut to a rectangular parallelepiped with 2.27(1) mm in the *c* direction, 1.51(1) mm in the $2b + a$ direction, and 1.47(1) mm in the *a* direction. The RUS data were obtained at different temperatures and magnetic fields in the 0.6- to 3.4-MHz range. The analysis was carried out with the RPR code [15,16] for ∼90 resonances and the polynomial order set to 12.

C. Mössbauer spectroscopy

Mössbauer spectra were obtained in a Janis Research SHI-850-5 cryostat with a spectrometer operating in constant acceleration mode and using a NaI(Tl) scintillation detector distributed by Ritverc GmbH. Less than 1 mg of the enriched, powdered sample was mixed with boron nitride and fixed with tape in a titanium sample holder. The velocity calibration of the spectrometer was performed with a 10-μm α-Fe foil; thus isomer shifts are reported relative to α-Fe at room temperature.

D. Nuclear inelastic scattering

Nuclear inelastic scattering (NIS) measurements were carried out at the high resolution dynamics beamline P01, PETRA III. This method provides direct access to the iron specific vibrational modes by probing the phonon assisted ^{57}Fe nuclear resonant absorption of ≈14.4-keV synchrotron radiation, monochromatized to meV resolution (see Ref. [17]). A layer of $\approx 5 \times 15\,\mathrm{mm}^2$ of the enriched powder was encapsulated between two strips of tape and fixed to the cold finger cryostat under grazing incidence. The energy resolution for the experiment was in the range of 0.8–1 meV. The iron partial density of phonon states (DPS) was extracted from the data using the program DOS [18].

III. RESULTS

A. Magnetometry

The $Mn_{5-x}Fe_xSi_3$ compounds with $1 \leqslant x \leqslant 4$ were investigated with vibrating sample magnetometry (VSM) in order to characterize the magnetic transitions and to assess the purity of the samples (see Fig. 2). The samples exhibit transitions to an ordered state at about 300 K, 200 K, 100 K, and 100 K, for $x = 4,3,2$, and 1, respectively. This observation is in agreement with literature values [19,20]. The absence of a ferromagnetic transition at about 300 K of $x = 1,2$, and 3 compounds indicates that no ferromagnetic impurities with $x = 4$ are present. The large magnetic moment in the $x = 4$

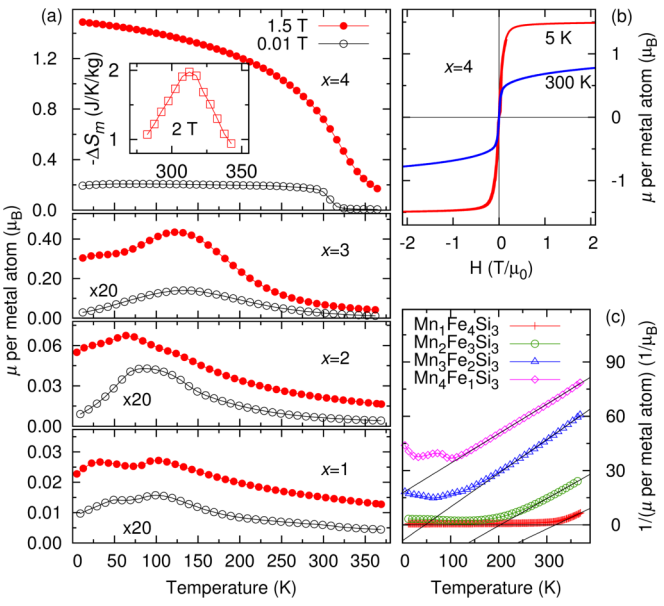

FIG. 2. (a) Magnetic moment μ per metal atom in $Mn_{5-x}Fe_xSi_3$ recorded in ZFC procedure. Selected 0.01-T measurements are scaled with a factor of 20, labeled in the plot where necessary. The magnetic entropy change for an applied field of 2 T for the $MnFe_4Si_3$ compound is depicted as an inset. (b) The hysteresis curve at 300 K and 5 K for the $MnFe_4Si_3$ compound. (c) The inverse moment, with black lines indicating the linear behavior in the paramagnetic region.

TABLE I. Weiss temperature θ and the effective paramagnetic moment μ_{eff} of $Mn_{5-x}Fe_xSi_3$ extracted from a Curie-Weiss fit of the VSM data at 0.01 T.

x	θ (K)	μ_{eff} (μ_B)
1	−62(2)	4.5(5)
2	128(4)	3.7(5)
3	216(10)	4.1(6)
4	314(8)	4.9(7)

phase prevents any detection of $x \leqslant 4$ impurities in this phase by means of VSM.

The recorded hysteresis data indicate a negative magnetic entropy change of 2 J/kg/K about the magnetic transition of $MnFe_4Si_3$ with an applied magnetic field of up to 2 T [see Fig. 2(a)]. As expected [21], the magnetic transition smears out using higher fields. The transition occurs over a large temperature range even in low fields (see Fig. 2). But the magnetic entropy change also appears over a broad temperature range of more than 50 K. The magnetic moment of $MnFe_4Si_3$ saturates with an applied field of ∼0.5 T at low temperatures [see Fig. 2(b)]. The hysteresis at 300 K indicates a reduced number of ordered moments and an additional linear contribution, likely related to induced paramagnetic moments. This observation indicates the coexistence of the ordered and the paramagnetic phase, as otherwise a continuous deformation of the hysteresis curve is expected about the transition.

Figure 2(c) depicts the inverse moment, exhibiting a linear increase with temperature in the paramagnetic phase. The intersection of the fit lines with the x axis provides the Weiss temperature θ, given in Table I. For ferromagnets, the Weiss and transition temperature are close but for antiferromagnets even the absolute value can differ significantly [21]. The effective moment in the paramagnetic region of these samples can be obtained from [21,22]

$$\mu_{\text{eff}} = \sqrt{\frac{\mu\ 3\ k_B\ (T-\theta)}{\mu_0\ H\ n}},$$

with μ the magnetic moment per atom, n the number of moment bearing atoms, and k_B the Boltzmann constant. The obtained effective moment, given in Table I, is in the range of 3.7–4.9 μ_B per metal atom for all samples. The saturated moment of the $MnFe_4Si_3$ compound in the ordered phase is ≈1.5 μ_B per atom [see Fig. 2(b)].

The likely origin for the total moment mismatch of the paramagnetic and the ordered phase is itinerant magnetism, as for this compound a mixed character of localized and itinerant magnetism is expected [23]. Furthermore, the observed moments match the Rhodes-Wohlfarth plot [24]. A detailed discussion with high-temperature data can be found in Refs. [8,9].

B. Resistivity measurements

The resistivity of $MnFe_4Si_3$ was investigated in order to assess the influence of the magnetic transition on the conduction electrons. Such effects could be important for the interpretation of the MCE. Temperature-dependent resistivity data were recorded parallel and perpendicular to the c axis with and without applied magnetic field (see Fig. 3). The observed absolute values agree with literature values on polycrystalline samples [25]. The temperature dependence of the resistivity has metallic character, however, without strictly linear behavior. The magnetic transition at ∼300 K leads to a change in slope of the resistivity in both crystallographic directions, whereas the applied magnetic field seems to have no influence on the temperature dependence.

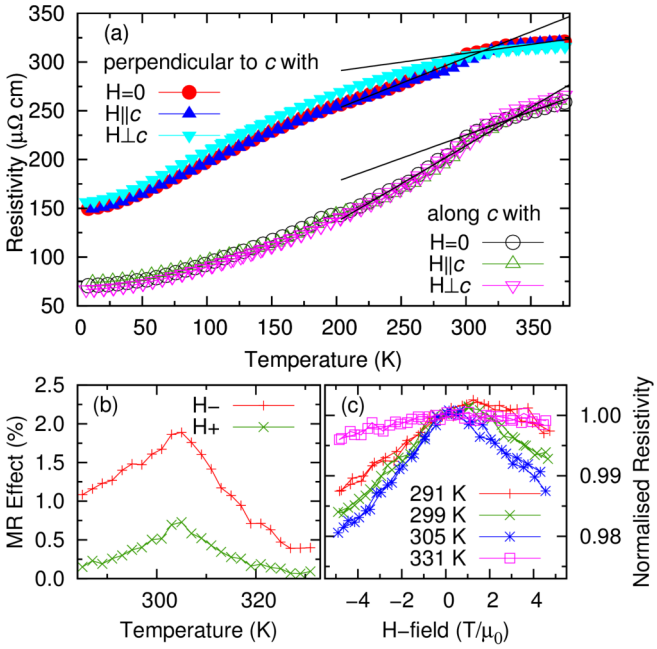

FIG. 3. Temperature-dependent resistivity of $MnFe_4Si_3$ single crystal in different directions, with 0 and 0.5 T magnetic field (a). The black lines illustrate the change in slope around the magnetic transition. The magnetoresistance in c direction with magnetic field perpendicular to c (b) is extracted from field-dependent resistivity measurements (c). H- indicates the extraction from the negative branch and H+ from the positive branch.

Significant magnetoresistance (MR) is only observed for transport in the c direction with an applied magnetic field perpendicular to c [see Figs. 3(b) and 3(c)]. The asymmetry of the obtained field-dependent curves is most likely due to an angle between the applied magnetic field and the spins. Due to the asymmetric shape, the analysis of the MR effect in Fig. 3(c) was performed for positive and negative branches separately. The maximal change of resistance under an applied field of +5 T and −5 T is given in Fig. 3(b). The observed MR effect of up to 2%, although not large compared to materials with giant magnetoresistance of ∼80%, is rather large for anisotropic magnetoresistance (see Ref. [26]).

C. Mössbauer spectroscopy

Mössbauer spectra of all compounds measured at 6 K are shown in Fig. 4. A temperature-dependent sequence for the $x = 4$ compound is depicted in Fig. 5.

Iron can occupy two different crystallographic sites in the $P6_3/mcm$ structural description. Using a simple sextet model

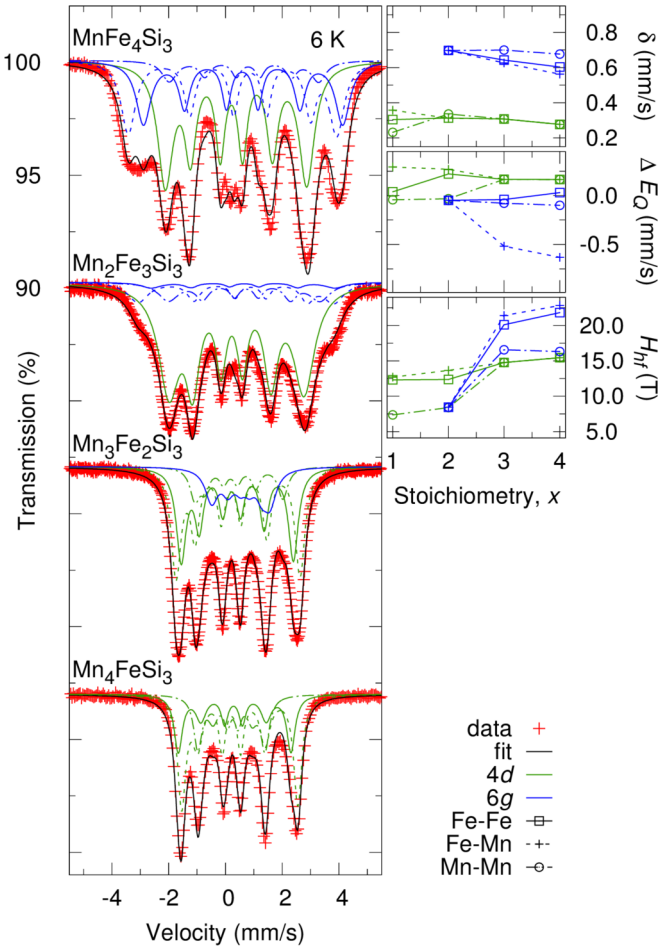

FIG. 4. Mössbauer spectra of $Mn_{5-x}Fe_xSi_3$ $1 \leqslant x \leqslant 4$ at 6 K (left) with the obtained spectral parameters (right). As the $x = 1$ compound exhibits almost no occupation of iron on the 6*g* site, it is thus fitted with the 4*d* site only.

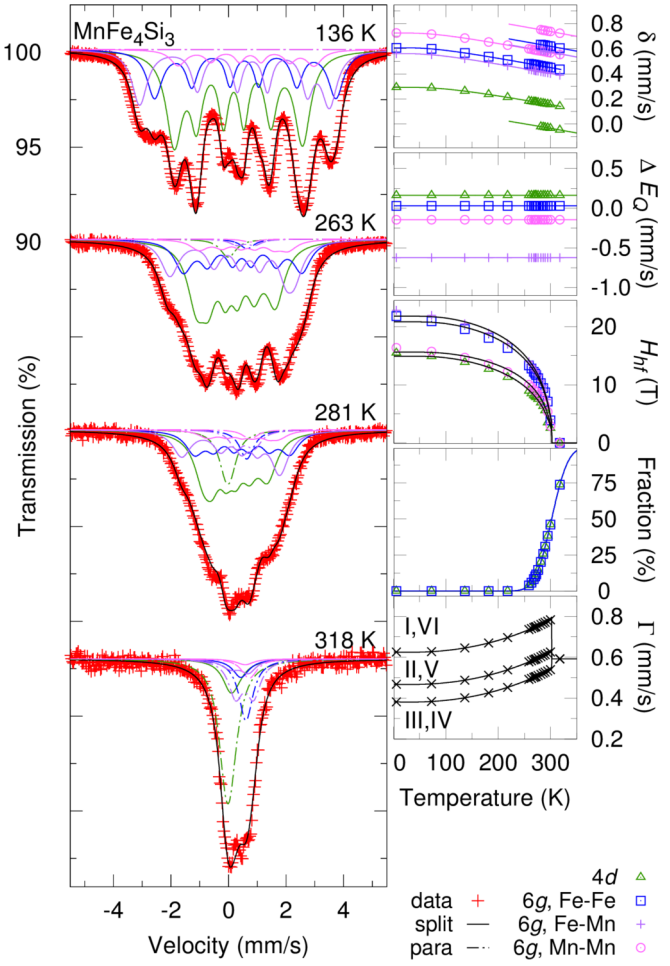

FIG. 5. Mössbauer spectra of $MnFe_4Si_3$ (left) and obtained temperature dependence of spectral parameters (right). The paramagnetic phase is illustrated with a dashed-dotted line and the magnetic split spectra with a continuous line. The linewidth Γ of peaks I–VI in the Mössbauer spectra are given separately in the magnetic ordered phase.

for each of the sites is, however, insufficient because the 4*d* and the 6*g* site have two nearest neighbors, which can be Fe, Mn, or both, leading to different hyperfine parameters. Consequently, Mössbauer spectra of each site with mixed occupation consist of at least three subspectra attributed to the following: Fe with two Mn neighbors; Fe with two Fe neighbors; and Fe with one Fe and one Mn neighbor, as sketched in Fig. 6.

In analogy to Ref. [27], the occupation of each site was modeled using a binomial distribution. Within this description, the relative amount $P(k)$ of the spectral component with k iron neighbors is related to the probability of iron occupation p by the formula:

$$P(k) = \frac{2}{k!(2-k)!} p^k (1-p)^{2-k}.$$

Starting values of p are calculated from crystallographic data [12]. The results of this binomial model, applied to the $x = 1,2$, and 3 data at 6 K, are depicted in Fig. 4 and the resulting areas of the spectral components are given in Table II.

The analysis of the $MnFe_4Si_3$ data was further improved by fitting all spectra for all temperatures simultaneously. Here, the adjusted parameters are not directly the hyperfine parameters of the probed atom but rather the temperature dependence of these parameters. In detail, the isomer shift was adjusted with the Debye model for the second-order Doppler shift [28] with

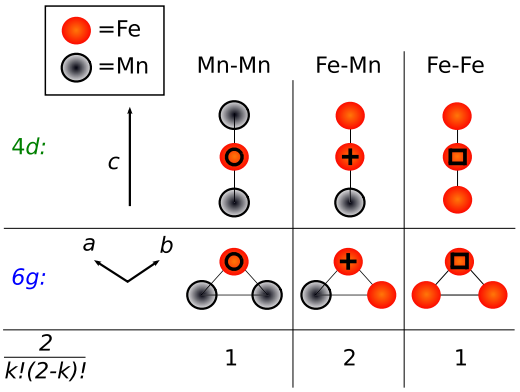

FIG. 6. A sketch illustrating the possible occupations of the 4*d* and 6*g* sites observed with Mössbauer spectroscopy, corresponding to the binomial model. The symbols (circle, cross, square) are chosen in accordance with Figs. 4 and 5.

TABLE II. The relative spectral areas obtained on the $Mn_{5-x}Fe_xSi_3$ series considering the statistically occupation of the two nearest neighbor positions. Values restricted by the model are given without errors.

	Spectral area		Binomial distribution	
x	$4d$	$6g$	p_{4d}	p_{6g}
4	0.45(1)	0.55(1)	1.00 (−)	0.64(2)
3	0.72(2)	0.28(2)	1.00 (−)	0.36(3)
2	0.86(1)	0.14(1)	0.68(1)	0.00(−)
1	1.00 (−)	0.00 (−)	0.51(1)	−

two adjustable parameters, the Mössbauer temperature [28] θ_M and the asymptotic limit at 0 K extrapolated from high temperatures δ_0. At the magnetic transition, the isomer shift was allowed to change by a step $\Delta\delta$, as also observed in Ref. [29]. The hyperfine magnetic field was fitted as an individual parameter for the $4d$ site and $6g$ site with two iron neighbors. The hyperfine fields of the other two nearest-neighbor arrangements are expressed in the model with a temperature-independent relative scaling with respect to the case of two iron nearest neighbors. The scaling factor for the arrangement with mixed manganese and iron neighbors was found to be

$$H_{hf}^{(\mathrm{Mn-Fe})}/H_{hf}^{(\mathrm{Fe-Fe})} = 1.047(2),$$

and with only manganese neighbors,

$$H_{hf}^{(\mathrm{Mn-Mn})}/H_{hf}^{(\mathrm{Fe-Fe})} = 0.75(1).$$

Finally, the measured hyperfine fields were fitted with the Bean and Rodbell model for a magnetic transition with magnetostriction exchange interactions. In accordance with this model, the hyperfine field is defined as [27]

$$H_{hf}(T) = H_0 * \sigma(T),$$

$$\sigma(T) = B_J\left(\frac{3J}{J+1}\frac{\sigma}{T/T_c}\left[1+\frac{3}{5}\frac{(2J+1)^4-1}{16(J+1)^3J}\eta\sigma^2\right]\right),$$

with scaling factor H_0, σ the reduced magnetization, B_J the Brillouin function [21] for the total moment J, T_c the critical temperature of the transition, and η a constant related to the shape of the $\sigma(T)$ curve, which is indicative of the order of the phase transition. The total moment was fixed to the value $J = 2$, as observed with magnetometry ($\mu_{\mathrm{eff}} = 2\sqrt{J(J+1)}$ [21], with $L = 0$). A free adjustment of this value led to strong numerical instability and was thus dismissed.

The quadrupole interaction turned out to be almost temperature independent, and thus ΔE_Q was assumed constant with temperature. The linewidth was observed to increase near the transition, in accordance with Ref. [14]. For a satisfactory adjustment, the linewidth needed to be described by a function of at least second order below the transition and a constant value above. It was further assumed that a coexistence of the paramagnetic and the ordered phase exists, with the relative amounts described by a Gaussian error function, similar to Ref. [27]. In all $x = 4$ spectra, a preferred orientation was observed, which leads to a ratio of the Mössbauer peaks of 3:1.7(1):1. The preferred orientation is likely related to the hexagonal structure of the series and was subsequently also introduced with success to the analysis of the $x = 1,2$, and 3 compounds. The obtained adjustment of the $x = 4$ compound is depicted in Fig. 5. The adjusted parameters are given in Table III.

TABLE III. Obtained values from the adjustment of the $MnFe_4Si_3$ data are presented. The θ_M and $\Delta\delta$ are equal for all $6g$ components.

		δ_0 (mm/s)	θ_M (K)	$\Delta\delta$ (mm/s)	ΔE_Q (mm/s)	$\mu_0 H_0$ (T)
$4d$		0.42(1)	460(50)	−0.19(1)	0.16(3)	14.9(2)
$6g$	Fe-Fe	0.70(1)	350(40)	0.17(1)	0.03(1)	20.8(2)
	Fe-Mn	0.66(1)	350(40)	0.17(1)	−0.62(1)	21.8(3)
	Mn-Mn	0.80(5)	350(40)	0.17(1)	−0.14(2)	15.61(2)

The results, obtained with the described model, reveal that the hyperfine magnetic field in the $Mn_{5-x}Fe_xSi_3$ series increases with increasing iron content (see Fig. 4). This effect is accompanied by increase of the transition temperature as observed by magnetometry (see Fig. 2). The average isomer shift of the individual sites stays nearly constant, but the average isomer shift of the sample increases with increasing iron content x due to increasing occupation of the $6g$ site. The strong change of the isomer shift of the $4d$ and $6g$ sites with the opposite sign at the transition is surprising, as such strong change in the isomer shift is often explained by a volume change affecting the electron density at the nucleus. However, the isomer shift should change with equal sign [29] and it was already mentioned that the volume changes only slightly about the transition [8,9].

The hyperfine field of the $4d$ site in $MnFe_4Si_3$ is only ≈75% of the value for the averaged $6g$ site (see Fig. 5). This relative value increases for decreasing iron content x (see Fig. 4).

In contrast to Ref. [13], almost no difference in the transition temperatures was observed for Fe on $4d$ and $6g$ sites and subsequently this temperature was constrained to the same value. The constrained fit results in a value of ∼302(5) K. The linewidth is increased for the outer peaks as compared to the inner ones, likely an effect of next nearest-neighbor interactions leading to an additional distribution of hyperfine fields. The importance of next nearest-neighbor interactions is not surprising, especially for the $6g$ site, in view of the interatomic distances given in the introduction.

The fit performed with the Bean and Rodbell model leads to a value of $\eta = 0.28(9)$ for the $4d$ site and a value of $\eta = 0.46(4)$ for the $6g$ site, indicative of a second-order transition. Note that $\eta = 0$ leads to a Brillouin function behavior, i.e., mean-field behavior, and a first-order transition requires $\eta > 1$, as observed in Ref. [27].

D. Nuclear inelastic scattering

In order to assess the influence of the magnetic transition on the lattice dynamics, ^{57}Fe nuclear inelastic scattering (NIS) was measured, yielding the partial density of phonon states (DPS) of the Fe sublattice.

The DPS of $MnFe_4Si_3$ obtained at different temperatures and magnetic fields are depicted in Fig. 7. No remarkable change takes place in the DPS at the magnetic transition around 300 K, apart from a softening of the phonon modes due to lattice expansion. A change in the DPS would be expected

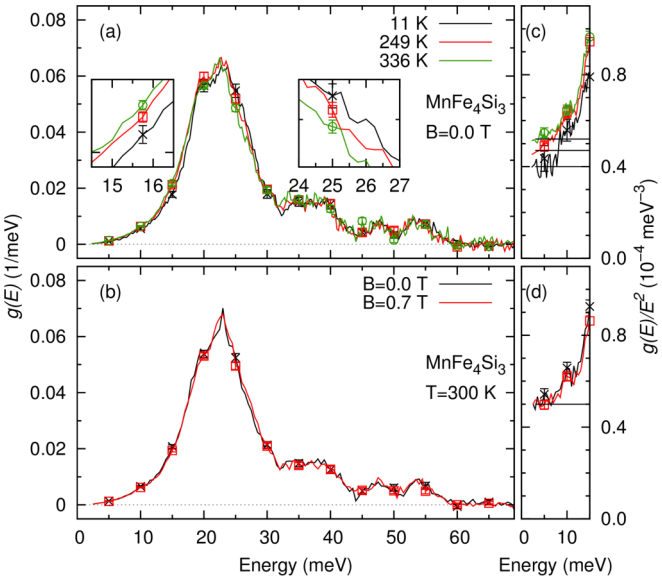

FIG. 7. Density of phonon states ($g(E)$) obtained in $MnFe_4Si_3$ at different temperatures (a) and different magnetic fields (b). The Debye levels of the reduced DPS, $g(E)/E^2$, are depicted with constant lines (c) and (d). The insets illustrate the regions with the largest observed phonon energy shifts. Error bars are given for every 20th data point.

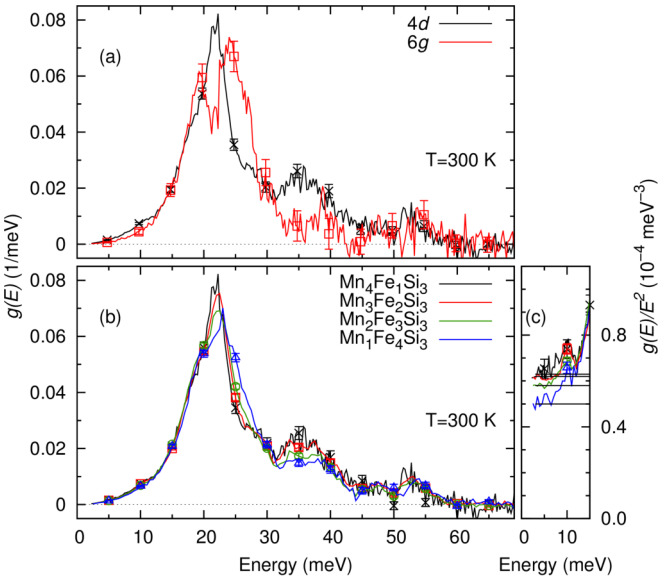

FIG. 8. The determined $4d$ and $6g$ specific DPS are plotted; the calculation is described in the text (a). The DPS of all investigated compounds of the $Mn_{5-x}Fe_xSi_3$ series at room temperature are depicted with a continuous change for increasing iron content (b).

for a magnetocaloric material and has been reported for $LaFe_{13-x}Si_x$ [30], revealing a shifting and strong broadening of the phonon modes across the transition.

The Debye level of the obtained DPS, defined as $\lim_{E\to 0}\frac{g(E)}{E^2}$, increases with increasing temperature (see Fig. 7). This observation is usual for lattice softening upon heating. Due to the subtraction of the elastic scattering line at zero energy, the obtained Debye level is only reliable above 3 meV. The Debye level is further used to extract the sound velocity [31] of the sample (see Table IV). Note that this procedure assumes a quadratic behavior of the DPS at low energies, also below 3 meV.

Similar to the temperature-dependent DPS, no direct influence of an external magnetic field on the lattice dynamics was observed [see Figs. 7(b) and 7(d)].

The phonon spectra of the $x = 1,2$, and 3 compounds of $Mn_{5-x}Fe_xSi_3$ series were also recorded at room temperature (see Fig. 8). The DPS gives access to a large number of physical properties [32,33], as summarized in Table IV. The mean force constant, the Lamb-Mössbauer factor, the vibrational contribution to the internal energy, and the vibrational entropy were found to be similar for the different compounds, as the slight dependence of the DPS on stoichiometry is insufficient to significantly change these parameters. In contrast, the sound velocity changes with composition.

TABLE IV. The calculated sound velocity v_s, Lamb-Mössbauer factor f, internal energy E_{int}, vibrational entropy S_{vib}, and mean force constant F_{mean}, obtained from the iron specific DPS of $Mn_{5-x}Fe_xSi_3$ at ~300 K. The given entropy is specific for the iron sublattice and neglects the other atoms.

$Mn_{5-x}Fe_xSi_3$	$x = 4$	$x = 3$	$x = 2$	$x = 1$
v_s (m/s)	3780(100)	3570(100)	3530(100)	3510(100)
f	0.77(2)	0.76(1)	0.76(1)	0.75(1)
E_{int} (meV)	84(7)	84(4)	89(5)	88(9)
S_{vib} (k_B/atom)	3.3(2)	3.3(1)	3.4(1)	3.4(2)
F_{mean} (N/m)	169(30)	168(20)	190(20)	178(40)

The vibrational entropy of the Fe sublattice in $MnFe_4Si_3$ is 300(20) J/kg/K, which is a first estimate for the overall vibrational entropy, as Fe constitutes half of the atoms and ≈60% of the mass. The recorded magnetic entropy change of 2 J/kg/K, which should be transferred to the vibrational entropy, is much smaller than S_{vib}. Thus, it is not surprising that no change of the DPS could be observed.

A site specific DPS can be estimated as the DPS obtained for Mn_4FeSi_3 solely represents the $4d$ site contributions. $6g$ site modes are calculated by

$$\text{DPS}_{6g} = 2\left(\text{DPS}_{\text{MnFe}_4\text{Si}_3} - \tfrac{1}{2}\text{DPS}_{\text{Mn}_4\text{FeSi}_3}\right),$$

due to the 1:1 ratio of the iron amount on $4d$ and $6g$ in $MnFe_4Si_3$. Both site specific DPS are depicted in Fig. 8(a). The different sites exhibit quite different phonon spectra, which leads to the observed change in the DPS for increasing iron content x, since the $6g$ becomes more prominent in the spectra.

Additional NIS studies on the $MnFe_4Si_3$ single crystal, relating the $4d$ and $6g$ modes to different crystallographic directions by utilizing the beam polarization [32,34], are provided in the Supplemental Material [10].

E. Resonant ultrasound spectroscopy

A $MnFe_4Si_3$ single crystal was investigated with resonant ultrasound spectroscopy (RUS) in order to assess the influence of the magnetic transition and of an applied magnetic field on the elasticity (see Fig. 9). Free-body resonance frequencies of the sample were recorded for different temperatures between

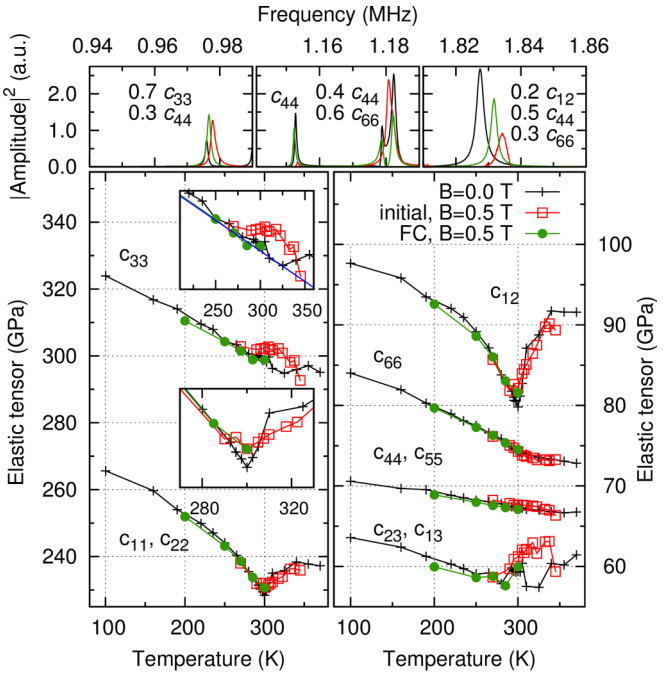

FIG. 9. Selected frequency ranges of RUS spectra at 300 K with the relative contribution of the elastic moduli to the corresponding resonances (top). Components of the elastic tensor extracted from RUS data upon changing temperature and magnetic field (bottom). The insets depict the transition region in detail. The procedures for the *initial* and the *FC* measurements are described in the text.

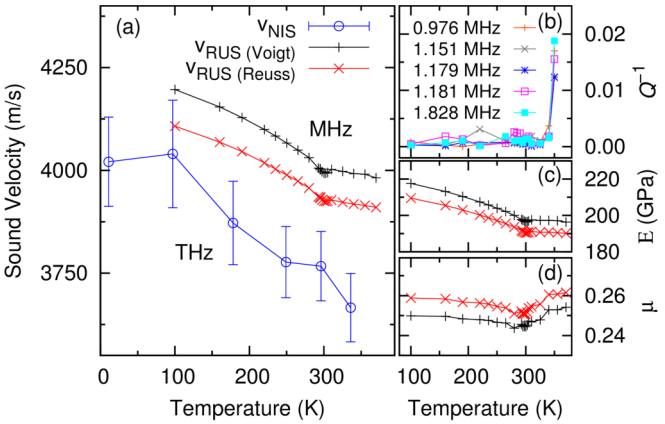

FIG. 10. Sound velocity in $MnFe_4Si_3$ obtained by RUS and NIS probing MHz and THz vibrations, respectively (a). The inverse quality factor is presented, for resonances shown in Fig. 9 (b). Young's modulus (c) and Poisson's ratio (d) determined within the Voigt and the Reuss approximation.

100 and 370 K without applied magnetic field. Then, an external magnetic field of 0.5 T was applied along c at room temperature and the *initial* data set was recorded upon heating. After reaching 350 K, the sample was field cooled (*FC*) to 200 K and the resonance frequencies were measured upon heating up to 300 K.

The elastic tensor of the hexagonal $MnFe_4Si_3$ single crystal consists of six different components, with the further restriction $c_{66} = (c_{11} - c_{12})/2$ leading to five independent moduli. The starting values for the fitting procedure were taken from the literature on the related Ta_5Si_3 compound [35].

The resonances were extracted for every temperature step individually. Afterwards, all results were compared and missing resonances, typically 5 out of 90 resonances, were identified so that for all temperatures and all magnetic fields a continuous behavior is observed as a function of temperature. This procedure is described in detail in Ref. [15]. The obtained values for the elastic tensor, with the Voigt notation, are depicted in Fig. 9. Only components c_{11},c_{22}, and c_{12} are strongly influenced by the magnetic transition, whereas c_{66} also exhibits a small change in slope around the transition. Components c_{23} and c_{13} are not very well determined, because only six of ≈90 resonance frequencies depend on these components with only up to 10%–30%.

The application of a magnetic field along the c axis mostly affects c_{11},c_{22}, and c_{12} (see inset). The observed change in c_{33} depends on the procedure for applying the magnetic field. For the first in-field measurement, the magnetic field was applied at 300 K and the sample was cooled down to 200 K for the measurements, which were recorded on heating. The second measurement was performed after field cooling the sample from 350 K to 200 K with an applied magnetic field of 0.5 T. Consequently, the first in-field measurement can be considered as zero-field cooled (ZFC), since the field was applied below or close to the transition. The second in-field measurement is a field cooled (FC) measurement, as the field was applied in the paramagnetic region. The deviation from the linear trend in the ZFC (*initial*) measurement of c_{33} could be related to additional stress due to the magnetic interaction. The spins, which lie in the ab plane [9], need to overcome the magnetocrystalline anisotropy in order to point along the c direction. This stress was probably not present in the paramagnetic and the FC phase, as indicated by the linear behavior of c_{33}. This effect is only visible in c_{33} and seems not to affect other components. Simultaneously, the c_{33} component is the longitudinal strain along the c direction, which is parallel to the applied magnetic field.

The root mean square (rms) value of the adjustment is between 0.2%–0.3% and the error on the moduli is about 3%. Thus, some measurements were repeated in order to examine the influence of the sample shape and the setup on the results. Different geometries typically lead to an error in the elastic moduli of about 2%. Different setups (changing piezoelectric crystal, holder, etc.) and re-mounting of the sample influence the results by less than 1%. Furthermore, the relative change of c_{11} and c_{22} on application of a magnetic field were verified to be trustworthy, because the good match with the zero-field data below 300 K (see inset of c_{11} and c_{22}) indicates an accuracy better than 1%.

Direct calculation of the averaged sound velocity in the sample is not possible due to the hexagonal structure. However, a lower and upper boundary can be obtained within Reuss and Voigt approximations, respectively [35,36]. The sound velocities obtained at different temperatures are depicted in Fig. 10 and compared with the sound velocities obtained by NIS.

Although some individual elements of the elastic tensor exhibit a strong, nonmonotonous change upon the magnetic transition, the averaged sound velocity *does not*. Only the different slope of the curve before and after transition indicates that an effect may take place. The sound velocities obtained at all temperatures are different compared to the NIS results.

The difference in the sound velocity indicates directly a difference in the Debye level, likely originating from the uncertainty of the NIS method below 3 meV. Thus, the Debye level (DL) is calculated from the sound velocity obtained with RUS using the formula in Ref. [31] and neglecting the ratio of resonant to averaged mass, because RUS is not isotope specific. It follows that

$$\mathrm{DL_{RUS}} = \frac{1}{2\pi^2\hbar^3 n v_{\mathrm{RUS}}^3} = 3.4(3) \times 10^{-5}\ \mathrm{meV}^{-3},$$

with atom density n. This $\mathrm{DL_{RUS}}$ can be used to replace the NIS data below 3 meV. The re-evaluation of the vibrational entropy [32] with the $\mathrm{DL_{RUS}}$ below 3 meV and the recorded DPS with NIS above 3 meV leads to the same result of $\approx$300 J/kg/K.

As mentioned above, the NIS results quantify only the iron sublattice entropy. The entropy of the whole system can be approximated by using the Debye model for the DPS and the obtained Debye level from RUS, yielding $\mathrm{DL_{RUS}} \times E^2$ as DPS and using the normalizing condition to define the cutoff energy. The calculation of the entropy in this model, with the same formula as applied to NIS [32], leads to $\approx$470(50) J/kg/K for the total vibrational entropy of the $MnFe_4Si_3$ compound at room temperature.

Young's modulus and Poisson's ratio can also be extracted from the elastic constants within the Voigt and Reuss approximation (see Fig. 10). The inverse quality factor $Q^{-1} = \Delta f/f$, which is related to the dissipation in the crystal, is also given in this plot. Young's modulus clearly mimics the behavior of the sound velocity, with a minor feature related to the magnetic transition. However, Poisson's ratio exhibits a different behavior with a nearly constant value below the transitions, an anomaly at the transition temperature, followed by an increase above the transition. This change in Poisson's ratio is in line with the anisotropic thermal expansion; see Ref. [9] or the Supplemental Material [10]. Furthermore, the stronger change above the transition relates to the dissipation, which also strongly increases. This change of both parameters indicates either a more complex behavior than the expected magnetic phase transition at room temperature or an anelastic process. Such a process could be Zener relaxation, which is a local relaxation process leading to a rearrangement of the atomic order or occupation. Furthermore, this relaxation is known to be very prominent in solid solutions [37]. Note that the strongly lowered quality factor is also one reason that the data is only analyzed for measurements up to $\approx$350 K, because broad, overlapping peaks impede an accurate extraction of their position.

IV. DISCUSSION

The magnetic behavior, resistivity and hyperfine parameters found in the $Mn_{5-x}Fe_xSi_3$ series are in agreement with earlier reports [14,19,38]. Magnetometry reveals that the magnetic moment per metal atom is similar in all four investigated compounds, whereas deviations from the phase diagram in Ref. [19] were observed. The $Mn_3Fe_2Si_3$ compound exhibits a positive Weiss temperature and should thus exhibit first a ferro- or ferrimagnetic transition, before entering the antiferromagnetic state.

The resistivity parallel and perpendicular to c is sensitive to the magnetic transition in $MnFe_4Si_3$ (see Fig. 3). The MR effect is only observed for transport along c and with a magnetic field in the ab plane. The effect takes place in a broad temperature range from 280 to 330 K and thus supports the broad transition found by Mössbauer spectroscopy and VSM on powder samples. Remarkably, the MR effect indicates an interaction between conduction electrons and magnetism, thus the electronic entropy might be influenced. Regarding the overall entropy, it is necessary to clarify how strongly the electronic entropy is changed by an applied field, in order to ensure that the magnetic entropy change yields a reliable estimation for the lattice entropy change and thus for the efficiency of the MCE.

An interesting feature of the Mössbauer data is the increase of the hyperfine field at both crystallographic sites with increasing iron content (see Fig. 4). The increase is most probably not related to a change of the total moment on changing iron content, as the effective moment of all four samples is similar. More likely, a change in bonding character on increasing iron content is the reason for the change in the hyperfine field. It has been already reported that the less electropositive iron forms more stable metal-metal bonds on the 4*d* site than manganese [14]. Thus, increasing iron content will change the overall bonding character of this site, as also reported for Fe_2P-type magnetocalorics [39].

A discontinuity in the isomer shift around the magnetic transition in $MnFe_4Si_3$ is observed (see Fig. 5). Such a strong change in isomer shift has been previously observed for other magnetocaloric materials [29]. Here, the change is in opposite directions for the 4*d* and 6*g* sites and thus probably not related to magnetostriction, but rather to a change of the bonding character or magnetic interaction. That the transition and thus the change in the isomer shift appears over a large temperature range might be explained by coexistence of the ordered and the paramagnetic phase. The coexistence of different phases could be originating in small deviations in the local occupation of the 4*d* and 6*g* site, distributed over the whole sample.

The magnetometry data reveal that the MCE exhibits a caretlike shape [see inset in Fig. 2(a)], an indication of a second-order magnetic transition [2]. The magnetic transition temperature does not shift but only smears out for increasing magnetic fields, also indicative of a second-order phase transition. The Bean and Rodbell model [40] used for analyzing the Mössbauer data yields $\eta_{4d} = 0.28 < 1$ and $\eta_{6g} = 0.46 < 1$ and thus also indicates a second-order transition with an exchange interaction influenced by the interatomic spacing.

The NIS data of selected $Mn_{5-x}Fe_xSi_3$ compounds reveal a hardening of the acoustic phonons and a softening of optical phonons for increasing iron content x. The unit cell volume is known to decrease with increasing iron content [14], whereby the ratio c/a exhibits a minimum between the $x = 2$ and $x = 3$

stoichiometry. Thus, a hardening of the lattice with increasing iron content is expected, as observed for the acoustic phonons. The simultaneously observed softening of the optical phonons [see Fig. 8(b)] must thus find a different explanation.

The DPS, extracted from NIS measurements at various temperatures and different magnetic fields, of $MnFe_4Si_3$ do not exhibit any strong change upon crossing the magnetic transition. The application of a magnetic field does not affect the DPS and cooling leads only to phonon hardening due to lattice contraction. Estimation of the vibrational entropy and the magnetic entropy change indicates that the Fe specific vibrational entropy changes by less than 1%, a change likely below the resolution limit of the NIS measurements. The effect of an entropy change will mainly influence the low energy acoustic phonons (see Ref. [32]). Thus, the low energy region, not completely accessible with NIS, must be further investigated in order to observe any possible change of the dynamics. However, these results do not directly imply that NIS is impractical for this purpose because the observation of a significant change in lattice entropy across the first-order transition in $LaFe_{13-x}Si_x$ has been previously reported [30].

RUS data, obtained in the MHz frequency range, thus probing much lower energetic phonons than NIS, exhibit changes in the dynamical properties around the magnetic transition. The *ab* plane components are strongly sensitive to the transition, i.e., c_{11},c_{22}, and c_{12}. This sensitivity solely in the *ab* plane to the transition was also observed for the lattice constants [9]. For illustration, the extracted excess strain from the lattice parameter data in Ref. [9] is presented in the Supplemental Material [10]. In addition to the temperature dependence, a smearing out of the transition region is observed with RUS under application of a magnetic field for the c_{11},c_{22}, and c_{12} components. These effects on the moduli indicate direct influence of the magnetic field on the elasticity. The observed effect cannot be explained with a simple volume change upon the magnetic transition due to the different behavior of different elastic constants and the ongoing change of the Poisson's ratio between 300 and 350 K. The observed behavior is uncommon for a second-order transition. The results in Ref. [9] also disagree with a strict second-order transition character. A possible explanation could be the presence of a Landau tricritical point. This interpretation would also explain the nonlinear recovery of the elastic constants below the transition due to the sixth-order term of the Landau expansion [41]. Nevertheless, this interpretation still fails to explain the different changes in the elastic behavior with temperature, as depicted in Fig. 10. These changes could be related to the possible Zener relaxation [37], increasing the dissipation at $\approx$350 K and may influence Poisson's ratio above the magnetic transition. In order to identify the origin of the increased dissipation at high temperatures, additional high-temperature ultrasound experiments would be useful. Likely, frequency- and concentration-dependent studies on the whole $Mn_{5-x}Fe_xSi_3$ series are most promising for such further investigations.

The sound velocities obtained from RUS and NIS, depicted in Fig. 10, are different. This discrepancy is not completely understood because other publications reported both methods to coincide [42,43] or to disagree [44], depending on the sample. In extracting sound velocities from NIS data it is assumed that a completely flat Debye level is present in the reduced DPS, i.e., a linear behavior of the phonon dispersion curve. This assumption could be inaccurate here for two reasons: first, the two methods operate in different frequency regions and thus different energies. The RUS method operates in the MHz region and thus directly in the linear branch of the phonon dispersion relation, whereas NIS operates on the THz scale. Consequently, if the linear approximation of the phonon dispersion curve is inaccurate, the estimated sound velocity will always be too small. Secondly, there could be a strong spin-phonon interaction in this material, as in Ref. [45]. The magnetism in $MnFe_4Si_3$ is anisotropic [8,9] and thus magnons start in the meV range [45,46]. Consequently, RUS measurements with MHz frequencies are too low in energy to observe a possible crossing of phonons and magnons. But, this energy scale is similar to NIS, which consequently would observe sound velocities influenced by phonon-magnon interactions.

V. CONCLUSION

Summarizing, Mössbauer spectroscopy and magnetometry carried out on the $Mn_{5-x}Fe_xSi_3$ series are in agreement with previous literature. Small deviations from the phase diagram of Ref. [19] were found but further dedicated experiments are needed in order to confirm these observations and to extract the magnetic structure of the series. The $Mn_3Fe_2Si_3$ compound appears to exhibit first a ferri- or ferromagnetic state before undergoing a transition to an antiferromagnetic state upon cooling.

The improved model for the analysis of the Mössbauer spectra, the VSM data, and also the single crystal resistivity measurements reveal a very broad temperature region of the magnetic transition, which is close to second order, according to the Bean and Rodbell model [40]. However, a typical second-order transition is not observed with RUS but rather a more complex behavior seems to be present. Also the strong temperature shift of the 4*d* and 6*g* isomer shift around the transition indicates a more complex behavior, e.g., a variance of the bonding character, because simple volume effects cannot explain that the electron density changes in opposite direction for the two sites.

The $MnFe_4Si_3$ solid solution exhibits magnetoelasticity and magnetoresistance around the magnetic transition. A magnetoelastic interaction is not observed in high energy phonons above 3 meV with NIS, neither on changing magnetic field nor on changing temperature. This observation contrasts with the low energy behavior for the sound waves in the MHz range, namely the elasticity probed with RUS, which indicates a strong interaction between lattice and magnetism. The RUS investigations reveal that only sound waves in the *ab* plane are sensitive to the magnetic transition and similar direction-dependent effects are observed in the resistivity. A discrepancy in the sound velocity was found by comparing NIS and RUS results and two possible scenarios are discussed. These scenarios are either a systematic deviation between NIS and RUS, due to a nonconstant Debye level, or, more likely, a strong phonon-magnon interaction, leading to a non-Debye-like behavior between 4 MHz and 0.75 THz (16 neV and 3 meV).

ACKNOWLEDGMENTS

R.P.H. acknowledges the Helmholtz Association of German Research Centers for funding VH NG-407 "Lattice dynamics in emerging functional materials" and support from the U.S. Department of Energy, Office of Science, Basic Energy Sciences, Materials Sciences and Engineering Division. Portions of this research were carried out at the light source PETRA III at DESY, a member of the Helmholtz Association (HGF). We would like to thank H.-C. Wille and K. Schlage for assistance in using beamline P01 and for support in analyzing the NIS data. We acknowledge helpful comments from M. Manley, J. Budai, and T. Watkins.

[1] E. Brück, J. Phys. D **38**, R381 (2005).

[2] K. A. Gschneidner Jr, V. K. Pecharsky, and A. O. Tsokol, Rep. Prog. Phys. **68**, 1479 (2005).

[3] V. Franco, J. Blázquez, B. Ingale, and A. Conde, Annu. Rev. Mater. Res. **42**, 305 (2012).

[4] E. Warburg, Ann. Phys. **249**, 141 (1881).

[5] W. F. Giauque and D. P. MacDougall, Phys. Rev. **43**, 768 (1933).

[6] N. A. de Oliveira and P. J. von Ranke, Phys. Rep. **489**, 89 (2010).

[7] V. K. Pecharsky and K. A. Gschneidner, J. Appl. Phys. **86**, 565 (1999).

[8] P. Hering, Master's thesis, RWTH Aachen, FZ Jülich, 2014.

[9] P. Hering, K. Friese, J. Voigt, J. Persson, N. Aliouane, A. Grzechnik, A. Senyshyn, and T. Brückel, Chem. Mater. **27**, 7128 (2015).

[10] See Supplemental Material at http://link.aps.org/supplemental/10.1103/PhysRevB.93.094304 for Additional Nuclear Inelastic Scattering studies on a $MnFe_4Si_3$ single crystal and direction dependent excess strain are presented.

[11] M. P. Annaorazov, S. A. Nikitin, A. L. Tyurin, K. A. Asatryan, and A. K. Dovletov, J. Appl. Phys. **79**, 1689 (1996).

[12] H. Bińczycka, v. Dimitrijević, B. Gajić, and A. Szytula, Phys. Status Solidi A **19**, K13 (1973).

[13] O. Gourdon, M. Gottschlich, J. Persson, C. d. l. Cruz, V. Petricek, M. A. McGuire, and T. Brückel, J. Solid State Chem. **216**, 56 (2014).

[14] V. Johnson, J. Weiher, C. Frederick, and D. Rogers, J. Solid State Chem. **4**, 311 (1972).

[15] A. Migliori and J. Sarrao, *Resonant Ultrasound Spectroscopy: Applications to Physics, Materials Measurements, and Nondestructive Evaluation* (John Wiley & Sons, New York, 1997).

[16] A. Migliori, J. Sarrao, W. M. Visscher, T. Bell, M. Lei, Z. Fisk, and R. Leisure, Physica B **183**, 1 (1993).

[17] R. Röhlsberger, *Nuclear Condensed Matter Physics with Synchrotron Radiation* (Springer, Berlin, 2004).

[18] V. Kohn and A. Chumakov, Hyperfine Interact. **125**, 205 (2000).

[19] L. Song, W. Dagula, O. Tegus, E. Brück, J. Klaasse, F. de Boer, and K. Buschow, J. Alloys Compd. **334**, 249 (2002).

[20] A. Candini, O. Moze, W. Kockelmann, J. M. Cadogan, E. Brück, and O. Tegus, J. Appl. Phys. **95**, 6819 (2004).

[21] S. Blundell, *Magnetism in Condensed Matter* (Oxford University Press, Oxford, 2001).

[22] J. M. D. Coey, *Magnetism and Magnetic Materials* (Cambridge University Press, Cambridge, 2010).

[23] T. Moriya and Y. Takahashi, Annu. Rev. Mater. Sci. **14**, 1 (1984).

[24] E. Wohlfarth, J. Magn. Magn. Mater. **7**, 113 (1978).

[25] R. Haug, G. Kappel, and A. Jaegle, J. Phys. Chem. Solids **41**, 539 (1980).

[26] P. A. Grünberg, Rev. Mod. Phys. **80**, 1531 (2008).

[27] R. P. Hermann, O. Tegus, E. Brück, K. H. J. Buschow, F. R. de Boer, G. J. Long, and F. Grandjean, Phys. Rev. B **70**, 214425 (2004).

[28] P. Gütlich, E. Bill, and A. X. Trautwein, *Mössbauer Spectroscopy and Transition Metal Chemistry* (Springer, Berlin, 2011).

[29] M. T. Sougrati, R. P. Hermann, F. Grandjean, G. J. Long, E. Brück, O. Tegus, N. T. Trung, and K. H. J. Buschow, J. Phys.: Condens. Matter **20**, 475206 (2008).

[30] M. E. Gruner, W. Keune, B. Roldan Cuenya, C. Weis, J. Landers, S. I. Makarov, D. Klar, M. Y. Hu, E. E. Alp, J. Zhao, M. Krautz, O. Gutfleisch, and H. Wende, Phys. Rev. Lett. **114**, 057202 (2015).

[31] M. Y. Hu, W. Sturhahn, T. S. Toellner, P. D. Mannheim, D. E. Brown, J. Zhao, and E. E. Alp, Phys. Rev. B **67**, 094304 (2003).

[32] R. Rüffer and A. Chumakov, Hyperfine Interact. **128**, 255 (2000).

[33] A. Chumakov and R. Rüffer, Hyperfine Interact. **113**, 59 (1998).

[34] D. Bessas, W. Tollner, Z. Aabdin, N. Peranio, I. Sergueev, H. Wille, O. Eibl, K. Nielsch, and R. P. Hermann, Nanoscale **5**, 10629 (2013).

[35] X. Tao, P. Jund, C. Colinet, and J.-C. Tedenac, Phys. Rev. B **80**, 104103 (2009).

[36] R. Hill, Proc. Phys. Soc. London, Sect. A **65**, 349 (1952).

[37] A. Nowick and B. Berry, *Anelastic Relaxation in Crystalline Solids* (Academic Press, Cambridge, 1972).

[38] K. Narasimhan, W. Reiff, H. Steinfink, and R. Collins, J. Phys. Chem. Solids **31**, 1511 (1970).

[39] N. H. Dung, Z. Q. Ou, L. Caron, L. Zhang, D. T. C. Thanh, G. A. de Wijs, R. A. de Groot, K. H. J. Buschow, and E. Brück, Adv. Energy Mater. **1**, 1215 (2011).

[40] C. P. Bean and D. S. Rodbell, Phys. Rev. **126**, 104 (1962).

[41] R. I. Thomson, T. Chatterji, C. J. Howard, T. T. M. Palstra, and M. A. Carpenter, J. Phys.: Condens. Matter **26**, 045901 (2014).

[42] D. Bessas, K. Z. Rushchanskii, M. Kachlik, S. Disch, O. Gourdon, J. Bednarcik, K. Maca, I. Sergueev, S. Kamba, M. Lezaić, and R. P. Hermann, Phys. Rev. B **88**, 144308 (2013).

[43] P. Bauer-Pereira, Structure and Lattice Dynamics of Thermoelectric Complex Chalcogenides, Ph.D thesis, University of Liège, Belgium, 2012.

[44] B. Klobes, M. Herlitschke, K. Z. Rushchanskii, H.-C. Wille, T. T. A. Lummen, P. H. M. van Loosdrecht, A. A. Nugroho, and R. P. Hermann, Phys. Rev. B **92**, 014304 (2015).

[45] W. Wettling, W. Jantz, and H. Dötsch, Applied Phys. **23**, 195 (1980).

[46] N. Ashcroft and D. Mermin, *Solid State Physics* (Cornell University Press, Cornell, 1976).